Alberto F. Maroto[1], Alejandro Barrallo-Gimeno[1,2], Jordi Llorens[1,2]

Differential role of type I and type II vestibular hair cells in two anti-gravity reflexes in the rat.

[1] Departament de Ciències Fisiològiques, Institut de Neurociències, Universitat de Barcelona, Feixa Llarga s/n, 08907 L'Hospitalet de Llobregat, Catalunya, Spain

[2] Institut d'Investigació Biomèdica de Bellvitge, IDIBELL, 08907 L'Hospitalet de Llobregat, Catalunya, Spain.

Corresponding autor: Prof. Jordi Llorens, Ph.D.; e-mail: jllorens@ub.edu; Ph: +34934024277

e-mail addresses and ORCID codes:

A.F.M.: amaroto7@ub.edu ; 0000-0001-8265-4902

A.B.G.: abarrallo@ub.edu ; 0000-0003-2086-8926

J.L.: jllorens@ub.edu ; 0000-0002-3894-9401

Word counts:

Abstract – 242

Introduction – 1046

Discussion – 1887

Number of tables – 0

Number of figures – 12

Abstract

The tail-lift reflex and the air-righting reflex in rats are anti-gravity reflexes that depend on vestibular function. To begin identifying their cellular basis, this study examined the relationship between reflex loss and the graded lesions caused in the vestibular sensory epithelia by varying doses of an ototoxic compound. After ototoxic exposure, we recorded these reflexes using slow motion video. The movies were used to obtain objective measures of these reflexes: the minimum angle formed by the nose, the back of the neck and the base of the tail during the tail-lift maneuver and the time to right in the air-righting test. The vestibular sensory epithelia were then collected from the rats and used to obtain type I (HCI), type II (HCII) and all hair cell (HC) counts in both central and peripheral parts of the crista, utricle, and saccule. As expected, tail-lift angles decreased and air-righting times increased in correlation with decreasing numbers of surviving HCs. However, for both functional measures, the degree of correlation varied with the cell type, zone and end-organ considered. We noted that the correlations of tail-lift angles were strikingly greater with HCI counts that HCII counts, greater with utricle and crista counts than saccule counts, and roughly similar with central/striola zones than peripheral zones. A similar HCI vs HCII difference was not recorded for air-righting times. We conclude that these two reflexes depend differently on HCI and HCII function and that the tail-lift angle reflects HCI function.

Keywords

Tail-lift reflex test. Air-righting reflex test. Type I hair cells. Type II hair cells. Vestibular epithelia. Rat. Ototoxicity.

INTRODUCTION

The vestibular system is the sensory system that provides perception of accelerations. As generated by gravity and movements of the body or the head alone, these accelerations can be linear or angular and of a wide diversity of magnitudes. The vestibular system allows for a precise encoding of this large variability of stimuli, thanks to the diversity of functional subsystems that it contains. These are based on the existence of diverse end-organs, types of transducing cells, primary afferent terminals, and physiological properties of the primary neurons (Desai et al, 2005a, 2005b; Eatock and Songer, 2011; Curthoys et al., 2017; Eatock, 2018).

In mammals, each inner ear has five vestibular sensory epithelia, one crista in each of three semicircular canals, and two maculae in the utricle and saccule (Fig 1A). In each of these end-organs, the cellular architecture defines a central zone, known as striola in the maculae, and a peripheral zone (Fig 1B). There are two types of sensory transducing cells, known as hair cells (HCs). Type I HCs (HCI) have an amphora-like shape, whereas type II HCs (HCII) are more cylindrical (Fig 1C). HCs are presynaptic to terminals of the afferent neurons of the vestibular ganglion. There are two types of terminals: calyx terminals encase HCI up to their neck, whereas HCII are contacted by standard bouton terminals. These two types of terminals define three types of afferents: calyx-only afferents that exclusively form calyx terminals in the central zones of the epithelia, bouton-only afferents, and dimorphic afferents that form both calyx terminals and bouton terminals. Physiologically, two types of afferents are recognized according to resting spike timing. Afferents from the peripheral zones of the receptors show highly regular timing, while afferents from the central crista or the striolar zone of the maculae are characterized by irregular spike timing. On stimulation, regular and irregular afferents show, respectively, tonic and transient responses. These diverse properties relate in a quite puzzling manner. Thus, irregular afferents are calyx-only or dimorphic and regular afferents are dimorphic or bouton-only, so both HCI and HCII provide input to both regular and irregular afferents. This arrangement greatly complicates the analysis of the roles played by the diverse zones and HC types in vestibular physiology. Nevertheless, an association between the functions of these features likely exists, because all of the irregular (center/striola) afferents receive input from HCIs and all regular (peripheral) afferents receive input from HCII (Eatock, 2018).

The vestibular information is used for a variety of purposes, including gaze stabilization, motor control and cognitive functions. The understanding of the precise role of each vestibular subsystem to each function is far from being complete. This includes a limited understanding of the substrate underneath vestibular dysfunction symptoms. To tackle these limitations, there is a need for multiple tests of vestibular function for which the anatomical, cellular, physiological, and molecular substrates are known, including the correspondence between human and animal measures. In clinical settings, testing of vestibular function is increasingly performed through the video head impulse test (vHIT) and assessment of the ocular and cervical vestibular-evoked myogenic potentials (oVEMP and cVEMP, respectively). All of these are measures of reflex responses elicited by fast stimuli. Thus, the vHIT test allows to individually test the six semicircular canals of the patient at high rotational accelerations that impede interference of the optokinetic reflex (Halmagyi et al., 2017). In the case of VEMPs, available evidence indicates that they reflect the function of irregular afferents from the striolar zone of the utricle (oVEMPs) or the saccule (cVEMPS) (Curthoys et al., 2012; Corneil and Camp, 2018; Curthoys et al., 2017, 2018; Ono et al., 2020).

In comparison to clinical tests, rodent tests of vestibular function remain underdeveloped. The best developed test is the evaluation of the vestibulo-ocular reflex (VOR), with most examples involving mice stimulated with low angular velocities (Beraneck et al., 2012; De Jeu and De Zeeuw, 2012; Imai et al., 2016). Another example is the recording of vestibular evoked potential responses to jerk stimuli in mice, recently shown to be defective in mice with compromised formation of the striolar/central zones (Ono et al., 2020). We have recently described the use of high-speed video recording to obtain objective and fully quantitative measures of two anti-gravitational reflexes in the rat, the tail-lift reflex, and the air righting reflex (Martins-Lopes et al., 2019). The first of these tests evaluates the trunk extension reflex shown by rats when lifted by the tail, by measuring the minimum angle formed by the nose, the back of the neck and the base of the tail during the lift maneuver. This reflex is lost in vestibular deficient animals, which show instead ventral curling, and therefore reduced angles (Hunt et al. 1987; Pellis et al., 1991). The second test evaluates the righting-in-the-air response by measuring the time taken by the head of the rat to right after the animal is released in supine position in the air to fall on a foam cushion. The role of vestibular input in this reflex is well documented (Pellis et al., 1989). Our previous study (Martins-Lopes et al., 2019) demonstrated that the minimum tail-lift angle and the air-righting time provide good measures of vestibular function loss following ototoxic insults. In the present study, we start establishing the cellular basis of these functional tests by studying the relationship between the vestibular dysfunction data and the loss of sensory HCs in the vestibular epithelia following the ototoxic insult. To gain insight into the contribution of the different HC types and epithelial zones to the reflexes, we separately counted HCI, HCII and all HCs in central/striolar zones and peripheral zones of all three vestibular end-organs. As expected, significant correlations were found between the functional measures and the HC counts. However, a striking difference in correlations was found comparing those between tail-lift angle and HCI and those between the angle and HCII counts. Tail-lift angles better correlated with crista and utricle counts than saccule counts, and similarly correlated with central/striola zones than peripheral zones. In contrast to the tail-lift reflex, the air-righting reflex did not show such a dissimilarity between correlations with HCI and HCII. This difference suggests that the tail-lift reflex mostly measures HCI, not HCII, function, so a simple non-invasive behavioral measure may be used to infer HCI function in the living rat.

RESULTS

Effects of IDPN ototoxicity on anti-gravity reflexes.

Rats exposed to IDPN showed effects on body weight, spontaneous behavior, tail-lift reflex, and air-righting reflex in accordance to previous observations (Crofton and Knight, 1991; Llorens et al., 1993; Martins-Lopes et al., 2019). The first experiment included rats exposed to 0, 400, 600 and 1000 mg/kg of IDPN and recorded dose- and time-dependent effects on the vestibular reflexes, as previously published elsewhere (Martins-Lopes et al., 2019). The findings for the tail-lift reflex were confirmed and extended in experiments 2, in which rats received 0, 400, 450, 500, 550 or 600 mg/kg of IDPN, and 3, in which animals were dosed over 3 consecutive days at 0, 3 x 150, 3 x 175, or 3 x 200 mg/kg·day (Supplementary Fig. S1). To obtain a single measure of the final effect of the ototoxic treatment on this reflex, we averaged the tail-lift angles from day 21 to the end of the experiment at days 28 (experiments 2 and 3) or 91 (experiment 1), as shown in Fig. 2A-C. The ventral curling of the vestibular-deficient rats results in low angles (Fig. 2D). ANOVA analysis of the averaged tail-lift angles for

experiments 1, 2, and 3 resulted, respectively, in F[3, 20] = 189.3 (p = 0.000), F[4, 20] = 7.296 (p = 0.001), and F [3, 17] = 13.44 (p = 0.000).

In agreement with the previous data on the effects of IDPN on the air-righting reflex (experiment 1, Martins-Lopes et al., 2019), a 3-day exposure to IDPN (experiment 3) was found to cause an impairment in performance resulting in dose- and time-dependent increases in air-righting times (Supplementary Fig. 2). Figure 2E-F show the average air-righting times from day 21 to the end of the experiment for experiments 1 and 3. ANOVA analysis of these averaged times resulted in F[3, 20] = 76.15 (p = 0.000), and F [3, 17] = 7.705 (p = 0.002), respectively.

Figure 2G shows the relationship between the tail-lift angles and the air-righting times obtained in individual animals. Tail-lift angles decreased before air-righting times increased. Thus, four of the six animals in the IDPN3X150 group had angles in the 80-120 range, below the normal range (>130 degrees), while their air-righting times were in the normal range (100 to 170 ms).

Dose-, epithelial zone-, and type-dependent loss of HCs after IDPN exposure.

The vestibular sensory epithelia of control rats (Fig. 3-6) showed the expected high density of HCs (Myo7a+), including HCI (identified by the Caspr+ calyx around the basolateral end) and HCII (with cytoplasmic calretinin label and no calyx). In the central or striola part of the receptors, most of the HCIs were contacted by calyx-only afferent terminals expressing calretinin. The shape of this calretinin label was very different from, and therefore not confused with, the cytoplasmic label of calretinin in HCII, which colocalizes with the myosin-VIIa label.

IDPN caused a dose-dependent loss of HCs as observed in previous studies (Llorens et al., 1993; Llorens and Demêmes, 1994; Martins-Lopes et al., 2019). The time course of the IDPN-induced HC degeneration has been well characterized, occurs mostly within one week after administration and is completed by three weeks (Llorens et al., 1993; Llorens and Demêmes, 1994; Seoane et al., 2001a). Therefore, the data collected represent the final result of the toxic lesion. While most of the samples from IDPN400 animals showed a control-like overall appearance (Fig 3B), vestibular epithelia from IDPN1000 animals showed no HCs, except for a few sparse HCII remaining in the saccule of 2 of the 6 animals. Other dose groups showed intermediate degrees of HC loss that varied as a function of HC type, receptor, and zone (Fig. 3C, D). For a quantitative analysis of these differences, counts of HCI (Caspr+), HCII (calretinin+) and all HCs (Myo7a+) were obtained from all the animals in the three behavioral experiments in seven different fields of observation: striola of the utricle, external periphery (lateral extra-striola) of the utricle, internal periphery (medial extra-striola) of the utricle, central crista , peripheral crista, striola of the saccule, and periphery of the saccule (Fig. 1B). The histological data of animals from the three behavioral experiments were analyzed as a single experiment as shown in figures 4, 5, and 6. Significant effects of IDPN were observed in all 21 ANOVA comparisons (all F[9, 53-59] > 7.98, p's = 0.000), but different dose response relationships were evident in different zones and cell type. For instance, a total loss of HCI was recorded in the central and peripheral crista of IDPN600 animals (Fig. 4), while comparison of this group with the Control group in the saccular periphery revealed a 50 % of survival of HCIs (Fig. 4) and no significant effect on HCII counts (Fig. 5). As another example, the fact that HCII counts in the saccular periphery were only reduced after the highest dose (1000 mg/kg) of IDPN (Fig. 5) clearly differed from the significant 33% decrease in HCI recorded already at the lowest one (400 mg/kg) in the striola of the utricle.

The numbers of HCs of each type and in each epithelial zone were estimated using a second antibody combination with samples from the second ear of the rats in the second and third experiment. In this combination, oncomodulin delineates the central/striola zone of the receptors. The data gathered (see supplementary material Fig. S3-S5), provided a confirmatory replicate of the different dose-response relationships that characterize different zones and cell types. Taken together, the two series of HC counts demonstrated that the sensitivity to the ototoxic treatment are consistent with the following differences: HCI >> HCII, crista = utricle > saccule, and center/striola ≥ periphery. In summary, HCI in the crista center zone and utricular striola were the most sensitive and HCII in the saccular periphery were the most resistant.

Correlation between HC loss and deficits in anti-gravity reflexes.

As a first step to identify the cellular basis of the tail-lift reflex and the air-righting reflex, we studied the correlations between the quantitative measures of the two vestibular reflexes evaluated in the present work and the HC counts. As shown in Fig. 7-12, the expected overall basic pattern was recorded: different doses of the ototoxic compound caused varying degrees of HC loss and these correlated with graded decreases in tail-lift angles and increases in air-righting times. However, the observed correlations varied as a function of the cell type, end-organ and epithelial zone considered.

As shown in Fig. 7, Pearson's correlation coefficients for the tail-lift angle were close or above 0.9 for HCI counts in the crista and utricle (both peripheral and central zones), and lower but > 0.7 for these cells in both zones of the saccule. In comparison, correlation coefficients were much lower between tail-lift angles and HCII counts (Fig. 8); these were below 0.6 but still significant for the crista and utricle and non-significant (below 0.1) for the two saccular areas. Except for the crista periphery, correlation coefficients between tail-lift angles and all HCs (Myo7a+, Fig. 9) were lower than those between angles and HCI counts.

The correlation between air-righting times and HCI counts are shown in Fig 10. Correlation coefficients varied between -0.73 and -0.87. The coefficients were much lower for HCII (Fig. 11) in both saccular zones, but still between -0.62 and -0.83 in the other vestibular areas. The correlation coefficients between air-righting time and all HCs (Fig. 12) varied between -0.567 and -0.883.

The correlations between the behavioral and histological data were also examined using the second series of immunochemical labels. As shown in Fig. S6 to S11, the results obtained with this second combination of antibodies were similar to those obtained with the first combination.

Synaptic puncta numbers in surviving HCII.

The comparisons of cell numbers shown above clearly indicated that HCI are more sensitive to IDPN toxicity than HCII. However, recent research demonstrates that functional loss may also be consequent to synaptic uncoupling before HC loss becomes evident (Sedó-Cabezón et al., 2015; Sultemeier and Hoffman, 2017; Cassel et al., 2019; Greguske et al., 2019). To evaluate the possibility that surviving HCII were suffering synaptic uncoupling, we assessed pre- and post-synaptic puncta numbers in cristae of animals selected to be representative of the different degrees of behavioral dysfunction. The results obtained (Supplementary Fig. S12) did not support that surviving HCII were suffering synaptic uncoupling. Thus, the number of pre-synaptic Ribeye puncta and of the post-synaptic PSD95 puncta were similar in HCII of control and IDPN-treated animals. Student's test t values were 0.138 for ribeye puncta and 0.403 for

PSD95 puncta, both $p > 0.05$ (20 d.o.f.). Also, no significant correlations were found between the number of synaptic puncta per HCII cell and the tail-lift angles ($r=-0.204$ for Ribeye, $r=-0.124$ for PSD95, both $p > 0.05$) or the air-righting times ($r=-0.346$ for Ribeye, $r=-0.201$ for PSD95, both $p > 0.05$).

DISCUSSION

The vestibular system operates in a large variety of frequency and intensity of inputs and encodes these diverse stimuli to be used in a large variety of reflex behaviors and motor control functions, as well as cognitive functions. The identification of the cellular basis of each vestibular function will contribute to our understanding of the biological roles of this system and contribute to our ability to confront vestibular deficits and diseases. In the present work, we have used a clinically relevant approach, exposure to an ototoxic compound, to cause diverse degrees of damage in the vestibular sensory epithelia, and then to establish the relationship between the degree of damage and the functional loss in two vestibular reflexes in the rat.

Because of the known difficulty in causing vestibular HC loss in rats with the most clinically relevant ototoxins, the aminoglycoside antibiotics (Granados and Meza, 2005), we used an experimental ototoxin whose effects show many similarities with those of the aminoglycosides. These include the progression of the damage in epithelium- and zone-dependent manners. Starting with the pioneering work by Lindeman (1969), the literature contains many references, including ours on IDPN (Llorens et al., 1993; Llorens and Demêmes, 1994), recognizing that HCI are more sensitive to ototoxic-induced degeneration than HCII, and that the susceptibility progresses in a crista > utricle > saccule order and from the central zones to the periphery of the receptors. However, surprisingly few studies have provided quantitative assessment of these differences (Lopez et al., 1997; Nakayama et al., 1996). In the present study, the data clearly demonstrated the higher susceptibility of HCI compared to HCII to IDPN ototoxicity, and the relative resistance of the saccule to this effect. In contrast, a similar susceptibility to the ototoxic damage was found between the crista and the utricle, and no clear differences were apparent between the central and peripheral regions. These apparent discrepancies may relate to methodological reasons (qualitative scanning electron microscopy analysis versus counts of immunolabelled HCs) as well as time course effects, as the greater sensitivity of the central zones seemed clear in terms of HCs degenerating at short times after exposure (Llorens and Demêmes, 1994; Seoane et al., 2001a). It must be also pointed out that in undamaged epithelia the density of HCs is lower in the central regions, and that the identification of these regions fades away when the HCI encased by calyx-only afferents that characterize the central/striola region are being lost. Therefore, it is not surprising that the ability to demonstrate small differences varies from method to method. In any case, the differential susceptibility of HCs of different types and epithelia to ototoxic damage is a well-established fact also known to occur in the auditory system. Thus, in the cochlea, inner HCs are more resistant to insults than outer HCs, and the susceptibility decreases progressively from its basal end to its apical end, resulting in the well-known features of clinical hearing loss, such as the predominant appearance of high-frequency loss. The precise basis of these differences is not established, but are believed to result from intrinsic biochemical and physiological differences among HCs (Lee et al., 2013; Fettiplace and Nam, 2019).

The HCI data presented here were obtained using Caspr1 as marker. Caspr1 does not label proper HCI, but the post-synaptic membrane in the inner side of their calyx afferents (Sousa et al., 2009; Lysakowski et al., 2011; Sedó-Cabezón et al., 2015). In previous studies, we have shown that this protein can be reversibly down-regulated during chronic IDPN toxicity, an exposure model in which HC detachment from the afferent terminals and synaptic uncoupling precedes HC degeneration (Sedó-Cabezón et al., 2015; Greguske et al., 2019). However, acute or sub-acute IDPN exposure causes irreversible HC degeneration (Llorens et al., 1994; Seoane et al., 2001a,b) and the stability of the behavioral effect recorded here matches this HC loss, not a reversible loss of Caspr1. Moreover, if there were HCI surviving in the epithelia without the Caspr1 label around them, we can assume that these were not providing physiologically useful signals to the vestibular pathway, as illustrated by the chronic toxicity model (Sedó-Cabezón et al., 2015; Greguske et al., 2019). HCII counts were obtained using the calcium binding protein calretinin as marker. Although the expression of calretinin has been reported to occur in only a fraction of HCII (Desai et al., 2005a, b), we found that virtually all HCII expressed it. Notwithstanding, the levels of expression were largely variable, and there were HCII expressing calretinin at levels low enough to be unnoticed in 4-color images or in other types of immunolabel imaging, but clearly identified in our confocal images after selection of the corresponding color channel.

Increasing the doses of the toxic compound administered to the animal expectedly resulted in more extensive damage and deeper functional loss. Significant correlations were thus logically found in many histological/behavioral comparisons. However, the fact that different regions and cell types of the vestibular epithelia showed different dose-response relationships allowed us to comparatively evaluate the correlations of the cell loss with the loss of the reflex responses. Although both the tail-lift and the air-righting reflexes are anti-gravity responses triggered by vestibular input, their different dependency on the IDPN dose (Fig. 2G) indicated that they may depend on different cellular substrates.

The correlations established between the number of HCI in crista and utricle and the decrease in tail-lift angles were very high, close or above 0.9, and clearly higher than those of HCII. In fact, observation of the data clouds in Figure 8 makes evident that tail-lift angles drop at lower doses than the doses at which HCII numbers start to decrease, while the relationships seen in Figure 7 between HCI and tail-lift angles are linear. This difference allows us to hypothesize that the tail-lift reflex provides an estimation of HCI, not HCII, function, and that the relationship between the angle and the number of surviving HCI is indeed linear. In further support of this conclusion, correlation coefficients of tail-lift angle versus HCI counts were in all cases but one (crista periphery) higher than with counts of all HCs, suggesting that no significant contribution of HCII input is involved in the reflex. Although the correlational nature of the present study impedes a firm conclusion, the data strongly support the hypothesis. A potential confounder for this conclusion would be that the HCII remaining in the sensory epithelia were in fact deafferented, so the loss of HCII input were larger than the loss of HCII cell bodies. However, we collected synaptic data that undermine this possibility.

In contrast to the tail-lift angle, the air-righting times showed maximum correlations with the number of all HCs in the central and peripheral areas of crista and utricle and the number of HCI in both areas of the saccule. Thus, except for the central and peripheral saccule, the number of all HCs better predicted performance in the air-righting reflex than the number of HCI or HCII alone. Looking at the data depicted in figure 10, it becomes apparent that only modest increases in air-righting times were recorded in animals showing a deep-to-complete

loss of HCI in the crista and utricle, and that these times still showed dose-dependent increase after complete loss of HCI in these receptors. These increases at higher doses better correlate with HCII loss in the crista and utricle and HCI loss in the saccule. Two hypotheses are congruent with these data. One is that the air-righting reflex depends mostly on the combined input from both HCI and HCII. The other is that it predominantly depends on input from saccular HCI. In discussing this point, we must also ponder the presence of an interfering factor in the assessment of the time to right, which is the contact with the foam pad. While all control rats righted themselves while in the air, many vestibular deficient rats did not attain the righting criterion until they were already on the foam. Therefore, the righting response of these animals was also driven by somatosensory information. However, this does not invalidate the observation of nearly normal air-righting in animals bearing a significant HCI loss.

The precise role of HCI and HCII in vestibular function has not been completely established yet. However, most evidence supports the notion that the HCI/calyx units are fast adapting receptors specializing in transduction of high frequency stimuli. These properties would serve to generate reflexes that drive fast compensatory actions required to respond to loss of balance, an hypothesis supported also by the fact that HCI-calyx units are an evolutionary innovation appearing in terrestrial vertebrates (Eatock, 2018). Nevertheless, such a simple interpretation does not completely integrate the well-established fact that the two types of physiologically defined afferents, irregular and regular, are associated to the zone they innervate (central/striolar and peripheral, respectively) rather than to type of cell (Goldberg, 2000). There are evidences that the two types of afferents provide two distinct channels encoding vestibular information in two different ways (Jamali et al., 2016), and that irregular/central afferents originate vestibulo-spinal (including vestibulo-collic) reflexes (Boyle et al., 1992). Also, a recent study has demonstrated that the centre/striola zones generate the vestibulo-evoked potential responses to jerk stimuli (Ono et al., 2020). The present study did not address the differential role of the two types of afferents on the tail-lift and air-righting reflexes, and the data gathered did not clearly discriminate between zones. Nevertheless, our results suggest ways for future studies to address these questions. For instance, more precise studies of the association of each component with each function as defined by pathological deficits may be designed using the constantly increasing knowledge of cell and afferent subtypes subdivided by zones as defined by the expression of unique proteins (McInturff et al., 2018; Hoffman et al., 2018). Also interesting would be to establish how graded loss of HCs modifies afferent physiology. To our knowledge, the impact of partial ototoxic lesions of the vestibular sensory epithelia on afferent responses has never been studied.

Another aspect in need of future research is the extrapolation to other species, most notably the mouse. In view of the known combinations of common features and species-specific differences in vestibular histology and physiology (Boyle et al., 1992; Curthoys et al., 2017; Desai et al., 2005a,b; Eatock, 2018; Goldberg, 2000), it would be premature to assume that a similar relationship between tail-lift angles and HC loss will occur in the mouse as in the rat. Although ventral curling during tail-lift has been reported in many vestibular-deficient mice, our observations after vestibular toxicity in rats (Llorens et al., 1993; Llorens and Rodríguez-Farré., 1997; Martins-Lopes et al., 2019; this study) and mice (Soler-Martin et al., 2007; Saldaña-Ruíz et al., 2013; Boadas-Vaello et al., 2017; Greguske et al., 2019) suggest that the abnormal tail-lift response develops more easily and robustly in the former than the latter species.

In summary, the present data supports the conclusion that different vestibulo-motor reflexes differentially depend on HCI and HCII function, and that some of them, such as the tail-lift reflex in rats, may predominantly depend on HCI function. One corollary of this conclusion is that the rat tail-lift data may more closely compare to human vHIT and VEMP data than the mouse low-velocity VOR data. Therefore, this work is of interest with respect to vestibular physiology but also opens new perspectives on the translational value of animal models of vestibular dysfunction.

MATERIAL AND METHODS

Animals and treatments

This study used three lots of male adult (8-9-week-old) Long-Evans rats (n=24, 25 and 24), obtained from Janvier Labs (Le-Genest-Saint-Isle, France). The animals were housed in groups of two or three in standard cages (215 x 465 x 145 mm) with wood shavings as bedding. Housing conditions were a 12:12 h light:dark cycle (07: 30-19:30 h), a temperature of 22 ºC ± 2ºC, and free access to food pellets (TEKLAD 2014, Harlan Laboratories, Sant Feliu de Codines, Spain). The rats were housed for acclimatization for six days before starting the experiments. During experiments, the animals were regularly weighed and evaluated for overall toxicity to limit suffering according to ethical criteria. The use of the animals was in accordance with EU Directive 2010/63, following Law 5/1995 and Act 214/1997 of the Generalitat de Catalunya, and Law 6/2013 and Act 53/2013 of the Gobierno de España. This included preceptive approval by the Ethics Committee on Animal Experimentation of the Universitat de Barcelona.

HC loss was induced by exposure to 3,3'-iminodipropionitrile (IDPN), a well characterized ototoxic compound (Crofton and Knigth, 1991; Llorens et al., 1993; Llorens and Demêmes, 1994; Crofton et al., 1994; Llorens and Rodríguez-Farré, 1997; Soler-Martín et al., 2007; Wilkerson et al., 2018). The first lot of animals was used in an experiment in which rats were administered a single dose of 0 (Control group), 400 (IDPN 400), 600 (IDPN 600), or 1000 (IDPN 1000) mg/kg of IDPN (>98%, TCI Europe, Zwijndrecht, Belgium), i.p., in 2 ml/kg of saline (n=6 / group). Behavioral and scanning electron microscopy data from this experiment have been published elsewhere (Martins-Lopes et al., 2019). For the present study, HC counts were obtained by immunofluorescent analysis from the second ear of these animals. In the second experiment, animals received 0, 450 (IDPN 450), 500 (IDPN 500), 550 (IDPN 550), or 600 mg/kg of IDPN (n=5/group). In the third experiment, rats were administered with 0, 150 (IDPN 3x150), 175 (IDPN 3x175), or 200 (IDPN 3x200) mg/kg·day of IDPN for 3 consecutive days (n=6/group). Administration of IDPN in three doses over three days has been reported to cause less toxicity than the administration of the cumulative dose in one single injection (Crofton and Knight, 1991). The animals were evaluated for vestibular function before exposure and at regular time-points after exposure for 13 weeks (experiment 1) or 4 weeks (experiments 2 and 3). The time-course data from experiment 1 (Martins-Lopes et al., 2019) indicated a stability in the reflex deficits between 4 and 13 weeks. The tail-lift reflex was assessed in the three lots of animals and the air-righting reflex was assessed only in experiments 1 and 3.

At the end of the experimental periods, rats were given an overdose of anesthesia and decapitated for the purpose of isolating the vestibular sensory epithelia. The temporal bones were immersed in cold fixative and immediately dissected under a fume hood. The first inner ear of animals in the first experiment was used for scanning electron microscopy as published

elsewhere (Martins-Lopes et al., 2019). The other inner ears were collected for the present study.

Assessment of vestibular reflexes

The tail-lift reflex and the air-righting reflex were assessed using high-speed video recording as described (Martins-Lopes et al, 2019). Briefly, in the tail-lift reflex test, the rat is grasped by the base of the tail, gently lifted to approximately 40 cm, and then lowered down to the starting point (see Supplementary movies A and B for the tail-lift reflex in control and vestibular deficient rats). To facilitate image tracking, a white marble is placed in the back of the neck of the rat with a rubber band collar and the test is done in front of a red background. In the air-righting reflex test, the experimenter holds the rat with the two hands in a supine position at approximately 40 cm of height and suddenly releases it to fall on a foam cushion (see Supplementary movies C and D for the air-righting reflex in control and vestibular deficient rats). The reflex behaviors were recorded at 240 frames per second with a Casio Exilim ZR700 or a GoPro Hero 5 camera. Using the free software Kinovea (www.kinovea.org) for video tracking, we obtained the coordinates of the nose, back of the neck and base of the tail at a 1/240 s frequency during the tail-lift maneuver, and the time from the release of the animal until it fully righted its head in the air-righting reflex test. A script in R programming language was then used to calculate the minimum angle from the nose-neck-tail coordinates during the tail-lift test (Martins-Lopes et al., 2019).

Immunohistochemistry

The following primary antibodies were used: rabbit anti-Myosin VIIa (Myo7a) from Proteus Biosciences (cat. # 25-6790), rabbit anti-tenascin from Millipore (cat. # AB19013), rabbit anti-oncomodulin from Swant (cat. # OMG4), guinea pig anti-calretinin from Synaptic Systems (cat. # 214-104), mouse anti-Myo7a (clone 138-1-s, IgG1, supernatant) from Developmental Studies Hybridoma Bank, mouse anti-CtBP2/Ribeye (clone 16/CtBP2, IgG1, cat. # 612044) from BD Biosciences, mouse anti-contactin-associated protein (Caspr1) (clone K65/35, IgG1, cat. # 75-001) and anti-PSD95 (clone K28/43, IgG2a, cat# 75-028) from Neuromab. We used the following secondary antibodies conjugated with Alexa Fluor fluorochromes: 488 goat anti-guinea-pig IgG H+L (catalog #A11073, Invitrogen/ThermoFisher), 555 donkey anti-rabbit IgGs H+L (#A-31572), 555 goat anti-mouse IgG2a (#A21137), 647 goat anti-mouse IgG1 (#A21240) and 654 donkey anti-mouse IgG H+L (catalog #A-21202). We also used the DyLight 405 donkey anti-rabbit IgG H+L (catalog #711-475-152, Jackson ImmunoResearch). The nuclear stain 4′,6-diamidino-2-phenylindole (DAPI) was obtained from Sigma.

Vestibular epithelia were dissected in cold 4 % freshly depolymerized paraformaldehyde in phosphate buffered saline (PBS). After dissection, the tissues were fixed for 1 h in the same fixative, transferred to a cryoprotective solution (34.5% glycerol, 30% ethylene glycol, 20% PBS, 15.5% distilled water) and stored at −20°C until further processing. For immunolabeling, we followed the protocol by Lysakowski et al. (2011). Briefly, samples were placed at room temperature, rinsed, permeabilized with 4% Triton X-100 in PBS (1 h) and blocked with 1% of fish gelatin in PBS containing 0,5% Triton X-100 (1 h). Primary antibodies were incubated in 0.1% Triton X-100 and 1% fish gelatin in PBS for 24h at 4°C. Samples from all animals were immunolabelled with rabbit anti-Myo7a (1/400), mouse anti-Caspr1 (1/400) and guinea-pig anti-calretinin (1/500). Samples from selected animals were also immunolabelled with mouse anti-Myo7a (1/100), rabbit anti-tenascin (1/200), rabbit anti-oncomodulin (1/400),

and guinea-pig anti-calretinin (1/500). To assess synaptic puncta, we combined the rabbit anti-Myo7a and the guinea pig anti-calretinin with the anti-CtBP2/Ribeye and anti-PSD95 antibodies. Secondary antibodies were incubated in the dark using the same buffer and conditions used with the primary antibodies. Specimens were thoroughly rinsed with PBS after each incubation period. When only three primary antibodies had been used, an incubation of 15 min with DAPI (1/1000) in PBS was intercalated among the final rinses. To assess synaptic contacts, the labeled specimens were included in a bloc of gelatin/albumin as described (Sedó-Cabezón et al., 2015) and sectioned at 40 μm in a vibrating blade microtome (Leica VT1000S). The whole epithelia or the epithelial sections were finally mounted in Mowiol medium.

Confocal microscopy, HC counts and synaptic counts.

Vestibular epithelia were visualized in a Zeiss LSM880 spectral confocal microscope using a 63× (NA: 1.4) objective. Z-stacks of optical sections 0,5 µm thick (for HC counts) or 0,3 µm thick (for synaptic counts) were obtained spanning the whole sensory epithelium. HC counts were obtained for images from one central/striolar region and one (crista and saccule) or two (utricle) peripheral regions (Fig. 1B). In the utricle, separate counts were obtained from the peripheral regions at the external (lateral) and internal (medial) sides of the striola. The obtained thick 3D images were processed with the blend option of the Imaris image processing software (Bitplane), and the resulting filtered images used for cell counts using the cell counter plugin of the ImageJ software (National Institute of Mental Health, Bethesda, Maryland, USA).

The first immunolabeling combination was used to obtain independent estimates of the numbers of HCs, HCIs and HCII. First, all HCs were identified by the cytoplasmic labeling of the anti-Myo7a antibody (Hasson et al., 1997). Second, the Caspr1 label of the calyceal junctions of the calyx afferents was used to count HCIs (Sousa et al., 2009; Lysakowski et al., 2011). As argued in the Discussion section below, this label provided a reliable identification of HCIs in the present model, in which HCs either degenerate or survive the toxic insult. Third, we counted cells with overlapping calretinin and myosin-VIIa cytoplasmic label as HCIIs (Dechesne et al., 1991). The calretinin label of calyx-only afferents in the central areas of the receptors is clearly distinguished from that of HCIIs (Desmadryl and Dechesne, 1992). In selected animals from the second and third lots, a second combination was used that included the anti-oncomodulin antibody as marker to prominently delineate the central zone of the receptors (Hoffman et al., 2018). With this combination, HCI from peripheral zones of the receptors were recognized by the tenascin expression at the calyceal junctions (Lysakowski et al., 2011). In the synaptic study, we counted numbers of pre-synaptic (ribeye) and post-synaptic (PSD-95) puncta on HCII defined by the co-labeling with the anti-Myo7a and anti-calretinin antibodies (Sedó-Cabezón et al., 2015; Greguske et al., 2019).

Statistics

Data are shown as mean +/- SE. Time course data were analyzed by repeated measures MANOVA (Wilk's criterion) with day as the within-subject factor. Other multiple group comparisons were performed using one-way ANOVA followed by Duncan's post-hoc tests. The Pearson coefficient was used to evaluate the correlation of pairs of data from the same animals. Student's t-test was used to compare synaptic count data. All analyses were done with the IBM SPSS 25 program package.

ACKNOWLEDGEMENTS

This study was supported by grants RTI2018-096452-B-I00 (Ministerio de Ciencia, Innovación y Universidades, Agencia Estatal de Investigación, Fondo Europeo de Desarrollo Regional, MCIU/AEI/FEDER, UE), and 2017 SGR 621 (Agència de Gestió d'Ajuts Universitaris i de Recerca, Generalitat de Catalunya). A.B.G is a Serra-Húnter fellow. The confocal microscopy studies were performed at the Scientific and Technological Centers of the University of Barcelona (CCiT-UB). We thank Dr. Benjamin Torrejon for technical assistance, and former students of the laboratory, Anna Bellmunt and Vanessa Martins-Lopes, for their contributions to the study. We also thank Drs. Ruth Anne Eatock and Kazuya Ono for their critical review of the manuscript.

COMPETING INTERESTS

None.

REFERENCES

Beraneck M, Bojados M, Le Séac'h A, Jamon M, Vidal PP (2012) Ontogeny of mouse vestibulo-ocular reflex following genetic or environmental alteration of gravity sensing. PLoS One 7: e40414. doi: 10.1371/journal.pone.0040414.

Boadas-Vaello P, Sedó-Cabezón L, Verdú E, Llorens J (2017) Strain and Sex Differences in the Vestibular and Systemic Toxicity of 3,3'-Iminodipropionitrile in Mice. Toxicol Sci 156: 109-122.

Boyle R, Goldberg JM, Highstein SM (1992) Inputs from regularly and irregularly discharging vestibular nerve afferents to secondary neurons in squirrel monkey vestibular nuclei. III. Correlation with vestibulospinal and vestibuloocular output pathways. J Neurophysiol 68: 471-484.

Cassel R, Bordiga P, Carcaud J, Simon F, Beraneck M, Le Gall A, Benoit A, Bouet V, Philoxene B, Besnard S, Watabe I, Pericat D, Hautefort C, Assie A, Tonetto A, Dyhrfjeld-Johnsen J, Llorens J, Tighilet B, Chabbert C (2019) Morphological and functional correlates of vestibular synaptic deafferentation and repair in a mouse model of acute-onset vertigo. Dis Model Mech 12(7). pii: dmm039115. doi: 10.1242/dmm.039115.

Corneil BD, Camp AJ (2018) Animal models of vestibular evoked myogenic potentials: The past, present, and future. Front Neurol 9: 489. doi: 10.3389/fneur.2018.00489.

Crofton KM, Knight T (1991) Auditory deficits and motor dysfunction following iminodipropionitrile administration in the rat. Neurotoxicol Teratol. 13: 575-581.

Crofton KM, Janssen R, Prazma J, Pulver S, Barone Jr.S (1994) The ototoxicity of 3,3'-iminodipropionitrile: Functional and morphological evidence of cochlear damage. Hear Res 80: 129-140.

Curthoys IS, Vulovic V, Manzari L (2012) Ocular vestibular-evoked myogenic potential (oVEMP) to test utricular function: neural and oculomotor evidence. Acta Otorhinolaryngol Ital. 32: 41-45.

Curthoys IS, Grant JW, Burgess AM, Pastras CJ, Brown DJ, Manzari L (2018) Otolithic receptor mechanisms for vestibular-evoked myogenic potentials: A review. Front Neurol 9: 366. doi: 10.3389/fneur.2018.00366.

Curthoys IS, MacDougall HG, Vidal P-P, de Waele C (2017) Sustained and transient vestibular systems: A physiological basis for interpreting vestibular function. Front Neurol 8: 117. doi: 10.3389/fneur.2017.00117.

De Jeu M, De Zeeuw CI (2012) Video-oculography in mice. J Vis Exp 65: e3971. doi: 10.3791/3971.

Dechesne CJ, Winsky L, Kim HN, Goping G, Vu TD, Wenthold RJ, Jacobowitz DM (1991) Identification and ultrastructural localization of a calretinin-like calcium-binding protein (protein 10) in the guinea pig and rat inner ear. Brain Res 560, 139-148

Desai SS, Zeh C, Lysakowski A. (2005a) Comparative morphology of rodent vestibular periphery. I. Saccular and utricular maculae. J Neurophysiol 93: 251–266.

Desai SS, Ali H, Lysakowski A (2005b) Comparative morphology of rodent vestibular periphery. II. Cristae ampullares. J Neurophysiol 93: 267–280.

Desmadryl G, Dechesne CJ (1992) Calretinin immunoreactivity in chinchilla and guinea pig vestibular end organs characterizes the calyx unit subpopulation. Exp Brain Res 89, 105-108.

Eatock RA (2018) Specializations for fast signaling in the amniote vestibular inner ear. Integr Comp Biol 58: 341–350.

Eatock RA, Songer JE (2011) Vestibular hair cells and afferents: two channels for head motion signals. Annu Rev Neurosci 34: 501–534.

Fettiplace R, Nam JH (2019) Tonotopy in calcium homeostasis and vulnerability of cochlear hair cells. Hear Res 376: 11-21.

Goldberg JM (2000) Afferent diversity and the organization of central vestibular pathways. Exp Brain Res 130: 277-297.

Granados O, Meza G (2005) Streptidine, a metabolic derivative produced after administration of streptomycin in vivo, is vestibulotoxic in rats. Histol Histopathol 20: 357-364.

Greguske EA, Carreres-Pons M, Cutillas B, Boadas-Vaello P, Llorens J (2019) Calyx junction dismantlement and synaptic uncoupling precede hair cell extrusion in the vestibular sensory epithelium during sub-chronic 3,3'-iminodipropionitrile ototoxicity in the mouse. Arch Toxicol 93: 417-434.

Hasson T, Gillespie PG, Garcia JA, MacDonald RB, Zhao Y, Yee AG, Mooseker MS, Corey DP (1997) Unconventional myosins in inner-ear sensory epithelia. J Cell Biol 137, 1287-1307.

Halmagyi GM, Chen L, MacDougall HG, Weber KP, McGarvie LA, Curthoys IS (2017) The video head impulse test. Front Neurol 8: 258. doi: 10.3389/fneur.2017.00258.

Hoffman LF, Choy KR, Sultemeier DR, Simmons DD (2018) Oncomodulin expression reveals new insights into the cellular organization of the murine utricle striola. J Assoc Res Otolaryngol 19, 33-51.

Hunt M.A., Miller S.W., Nielson H.C., Horn K.M. (1987) Intratympanic injections of sodium arsanilate (atoxil) solution results in postural changes consistent with changes described for labyrinthectomized rats. Behav Neurosci 101, 427–428.

Imai T, Takimoto Y, Takeda N, Uno A, Inohara H, Shimada S (2016) High-speed video-oculography for measuring three-dimensional rotation vectors of eye movements in mice. PLoS One 11: e0152307. doi: 10.1371/journal.pone.0152307.

Jamali M, Chacron MJ, Cullen KE (2016) Self-motion evokes precise spike timing in the primate vestibular system. Nat Commun 7: 13229. doi: 10.1038/ncomms13229

Lee JH, Park C, Kim SJ, Kim HJ, Oh GS, Shen AH, So HS, Park R (2013) Different uptake of gentamicin through TRPV1 and TRPV4 channels determines cochlear hair cell vulnerability. Exp Mol Med 45: e12. doi: 10.1038/emm.2013.25.

Lindeman H.H. (1969) Regional differences in sensitivity of the vestibular sensory epithelia to ototoxic antibiotics. Acta Otolaryngol 67: 177-189.

Llorens J, Demêmes D (1994) Hair cell degeneration resulting from 3,3'-iminodipropionitrile toxicity in the rat vestibular epithelia. Hear Res 76: 78-86.

Llorens J, Demêmes D, Sans A (1993) The behavioral syndrome caused by 3,3'-iminodipropionitrile and related nitriles in the rat is associated with degeneration of the vestibular sensory hair cells. Toxicol Appl Pharmacol 123: 199-210.

Llorens J, Rodríguez-Farré E (1997) Comparison of behavioral, vestibular, and axonal effects of subchronic IDPN in the rat. Neurotoxicol Teratol 19: 117-127.

Lysakowski A, Gaboyard-Niay S, Calin-Jageman I, Chatlani S, Price SD, Eatock RA (2011) Molecular microdomains in a sensory terminal, the vestibular calyx ending. J Neurosci 31: 10101-10114.

Lopez I, Honrubia V, Lee S.C., Schoeman G, Beykirch K (1997) Quantification of the process of hair cell loss and recovery in the chinchilla crista ampullaris after gentamicin treatment. Int J Dev Neurosci 15: 447-461.

Martins-Lopes V, Bellmunt A, Greguske EA, Maroto AF, Boadas-Vaello P, Llorens J (2019) Quantitative assessment of anti-gravity reflexes to evaluate vestibular dysfunction in rats. J Assoc Res Otolaryngol 20: 553-563.

McInturff S, Burns JC, Kelley MW (2018) Characterization of spatial and temporal development of Type I and Type II hair cells in the mouse utricle using new cell-type-specific markers. Biol Open 7: bio038083. doi: 10.1242/bio.038083.

Nakayama M, Riggs LC, Matz GJ (1996) Quantitative study of vestibulotoxicity induced by gentamicin or cisplatin in the guinea pig. Laryngoscope. 106: 162-167.

Ono K, Keller J, López Ramírez O, González Garrido A, Zobeiri OA, Chang HHV, Vijayakumar S, Ayiotis A, Duester G, Della Santina CD, Jones SM, Cullen KE, Eatock RA, Wu DK. (2020) Retinoic acid degradation shapes zonal development of vestibular organs and sensitivity to transient linear accelerations. Nat Commun 11: 63. doi: 10.1038/s41467-019-13710-4.

Pellis SM, Pellis VC, Morrissey TK, Teitelbaum P (1989) Visual modulation of vestibularly-triggered air-righting in the rat. Behav Brain Res 35: 23-26.

Pellis S.M., Pellis V.C., Teitelbaum P. (1991) Labyrinthine and other supraspinal inhibitory controls over head-and-body ventroflexion. Behav Brain Res. 46: 99-102.

Saldaña-Ruíz S, Boadas-Vaello P, Sedó-Cabezón L, Llorens J (2013) Reduced systemic toxicity and preserved vestibular toxicity following co-treatment with nitriles and CYP2E1 inhibitors: a mouse model for hair cell loss. J Assoc Res Otolaryngol 14: 661-671.

Sedó-Cabezón L, Jedynak P, Boadas-Vaello P, Llorens J (2015) Transient alteration of the vestibular calyceal junction and synapse in response to chronic ototoxic insult in rats. Dis Model Mech 8: 1323-1337.

Seoane A, Demêmes D, Llorens J (2001a). Relationship between insult intensity and mode of hair cell loss in the vestibular system of rats exposed to 3,3'-iminodipropionitrile. J Comp Neurol 439: 385-399.

Seoane A, Demêmes D, Llorens J (2001b). Pathology of the rat vestibular sensory epithelia during subchronic 3,3'-iminodipropionitrile exposure: hair cells may not be the primary target of toxicity. Acta Neuropathol 102: 339-348.

Soler-Martín C, Diez-Padrisa N, Boadas-Vaello P, Llorens J (2007) Behavioral disturbances and hair cell loss in the inner ear following nitrile exposure in mice, guinea pigs, and frogs. Toxicol Sci 96: 123-132.

Sousa AD, Andrade LR, Salles FT, Pillai AM, Buttermore ED, Bhat MA, Kachar B (2009) The septate junction protein caspr is required for structural support and retention of KCNQ4 at calyceal synapses of vestibular hair cells. J Neurosci 29: 3103-3108.

Sultemeier DR, Hoffman LF (2017) Partial aminoglycoside lesions in vestibular epithelia reveal broad sensory dysfunction associated with modest hair cell loss and afferent calyx retraction. Front Cell Neurosci 11: 331. doi: 10.3389/fncel.2017.00331.

Wilkerson BA, Artoni F, Lea C, Ritchie K, Ray CA, Bermingham-McDonogh O (2018) Effects of 3,3'-iminodipropionitrile on hair cell numbers in cristae of CBA/CaJ and C57BL/6J Mice. J Assoc Res Otolaryngol 19: 483-491.

FIGURE LEGENDS

Figure 1. A. Schematic drawing of the mammalian inner ear, showing the five vestibular sensory epithelia, three cristae, the utricle and the saccule. B. In each vestibular epithelia a central zone (named striola for the utricle and saccule) can be differentiated from the peripheral zones by several histological and physiological criteria. Squares show the approximate size and location of the seven areas imaged for cell counting: crista center, crista periphery, utricle periphery external (lateral) to the striola, utricle striola, utricle periphery internal (medial) to the striola, saccule striola and saccule periphery. C. Cell types, afferent terminals and structural characteristics of the vestibular epithelium. The epithelium consists of type I hair cells (HCI), type II hair cells (HCII) and supporting cells (sc). Calyceal junctions characterize the contacts between HCIs and the calyx terminals encasing them. HCII are contacted by bouton terminals. There are three type of afferents: dimorphic (DM), forming both calyx and bouton terminals, calyx-only (CO) and bouton-only (BO) afferents. Calyx-only afferents characterize the central/striola regions. The HCs contain pre-synaptic structures (seen as puncta when immunolabelled) and the afferents contain post-synaptic densities (post-synaptic pucta).

Figure 2. Effects of the vestibular toxicity of IDPN on the tail-lift and air-righting reflexes. (A-C) Mean $\pm$ SE minimum nose-neck-base of the tail angles displayed by the rats when lifted by the tail and lowered back.). (D) Schematic drawing of the tail-lift angle as obtained from a rat suffering a deep loss of vestibular function. (E-F) Mean $\pm$ SE air-righting times displayed by the rats when dropped in supine position from approximately 40 cm above a foam cushion. The data are average values from days 7 to 91 after exposure (A and E, 0 - 1000 mg/kg, one dose, n=6/group) or days 7 to 28 after exposure (B and F, 0 - 200 mg/kg·day, for 3 consecutive days, n=6/group; and C, 0 - 600 mg/kg, one dose, n=5/group). (G) Relationship between individual values of the tail-lift angle and the time to right in the animals whose group values are shown in panels A, B, E and F. *: $p<0.05$, significantly different from control group, Duncan's test after significant ANOVA.

Figure 3. Effect of ototoxic exposure on the density of sensory hair cells (HCs) in the vestibular epithelia. The example images correspond to the medial part of the utricle, peripheral to the striola. Type I HCs (HCI) are revealed by the Caspr+ label on the inner membrane of the afferent calyx terminal (green). Type II HCs (HCII) show no Caspr+ label but are Myo7a+ (red) and calretinin+ (white). Nuclei were labeled with DAPI (blue). Images shown here are stack projections optimized to provide an overall sense of HC density, not an accurate identification of the cell types. Cells that seem to be Myo7+, Caspr- and calretinin- may be HCII that express calretinin at low levels or HCI with their calyceal junction in planes not included in the image. Also, HC superposition generates apparent calretinin label in Caspr1+ cells. For cell counts, types were unambiguously identified as shown in Fig. 4-6. (A) Normal density of cells in a control rats. (B) Control-like appearance was found in most rats receiving the lowest dose of IDPN (400 mg/kg). (C) Overt loss of HCI and HCII in a utricle of a rat dosed with 500 mg/kg of IDPN. (D) Complete loss of HCI and nearly complete loss of HCII in a rat dosed with 600 mg/kg of IDPN. Scale bars = 30 μm.

Figure 4. Differences in the loss of type I hair cells (HCI) after exposure to the ototoxic compound, IDPN, as a function of the dose (400 to 1000 mg/kg, see legend), zone (central/striola vs periphery) and end-organ (utricle, crista and saccule). Note that loss of HCI starts at low doses of IDPN. The images in the upper-left corner show the use of the Caspr label (green) to identify HCI. Scale bars = 10 μm. Bar graphs show HCI counts (X$\pm$SE) according

to end-organ, region within it and IDPN dose. Numbers below the bars indicate numbers of animals. *: $p<0.05$, significantly different from control group, Duncan's test after significant ANOVA.

Figure 5. Differences in the loss of type II hair cells (HCII) after exposure to the ototoxic compound, IDPN, as a function of the dose (400 to 1000 mg/kg, see legend), zone (central/striola vs periphery) and end-organ (utricle, crista and saccule). Note that the lower doses of IDPN have no effect on HCII counts, particularly in the saccule. The images in the upper-left corner show the use of the Myo7a (red) and calretinin (white) labels to identify HCII. Scale bars = 10 μm. Bar graphs show HCII counts ($X \pm SE$) according to end-organ, region within it and IDPN dose. Numbers below the bars indicate numbers of animals. *: $p<0.05$, significantly different from control group, Duncan's test after significant ANOVA.

Figure 6. Differences in the loss of all hair cells (HC) after exposure to the ototoxic compound, IDPN, as a function of the dose (400 to 1000 mg/kg, see legend), zone (central/striola vs periphery) and end-organ (utricle, crista and saccule). The images in the upper-left corner show the use of the Myo7a (red) label to identify HCs. Scale bars = 10 μm. Bar graphs show HC counts ($X \pm SE$) according to end-organ, region within it and IDPN dose. Numbers below the bars indicate numbers of animals. *: $p<0.05$, significantly different from control group, Duncan's test after significant ANOVA.

Figure 7. Relationship between HCI loss and tail-lift angle decrease after exposure to a variety of doses of the ototoxic compound, IDPN, as a function of the zone (central/striola vs periphery) and end-organ (utricle, crista and saccule). Individual data shown here correspond to those shown as group means in Fig. 2A-C (angles) and Fig. 4 (HCI counts). On each panel, the Pearson's correlation coefficient (r) and its level of statistical significance (p) are shown.

Figure 8. Relationship between HCII loss and tail-lift angle decrease after exposure to a variety of doses of the ototoxic compound, IDPN, as a function of the zone (central/striola vs periphery) and end-organ (utricle, crista and saccule). Individual data shown here correspond to those shown as group means in Fig. 2A-C (angles) and Fig. 5 (HCII counts). On each panel, the Pearson's correlation coefficient (r) and its level of statistical significance (p) are shown.

Figure 9. Relationship between all HC loss and tail-lift angle decrease after exposure to a variety of doses of the ototoxic compound, IDPN, as a function of the zone (central/striola vs periphery) and end-organ (utricle, crista and saccule). Individual data shown here correspond to those shown as group means in Fig. 2A-C (angles) and Fig. 6 (all HC counts). On each panel, the Pearson's correlation coefficient (r) and its level of statistical significance (p) are shown.

Figure 10. Relationship between HCI loss and air-righting time increase after exposure to a variety of doses of the ototoxic compound, IDPN, as a function of the zone (central/striola vs periphery) and end-organ (utricle, crista and saccule). Individual data shown here correspond to those shown as group means in Fig. 2E-F (times) and Fig. 4 (HCI counts). On each panel, the Pearson's correlation coefficient (r) and its level of statistical significance (p) are shown.

Figure 11. Relationship between HCII loss and air-righting time increase after exposure to a variety of doses of the ototoxic compound, IDPN, as a function of the zone (central/striola vs periphery) and end-organ (utricle, crista and saccule). Individual data shown here correspond to those shown as group means in Fig. 2E-F (times) and Fig. 5 (HCII counts). On each panel, the Pearson's correlation coefficient (r) and its level of statistical significance (p) are shown.

Figure 12. Relationship between all HC loss and air-righting time increase after exposure to a variety of doses of the ototoxic compound, IDPN, as a function of the zone (central/striola vs periphery) and end-organ (utricle, crista and saccule). Individual data shown here correspond to those shown as group means in Fig. 2E-F (times) and Fig. 6 (all HC counts). On each panel, the Pearson's correlation coefficient (r) and its level of statistical significance (p) are shown.

Figure 1

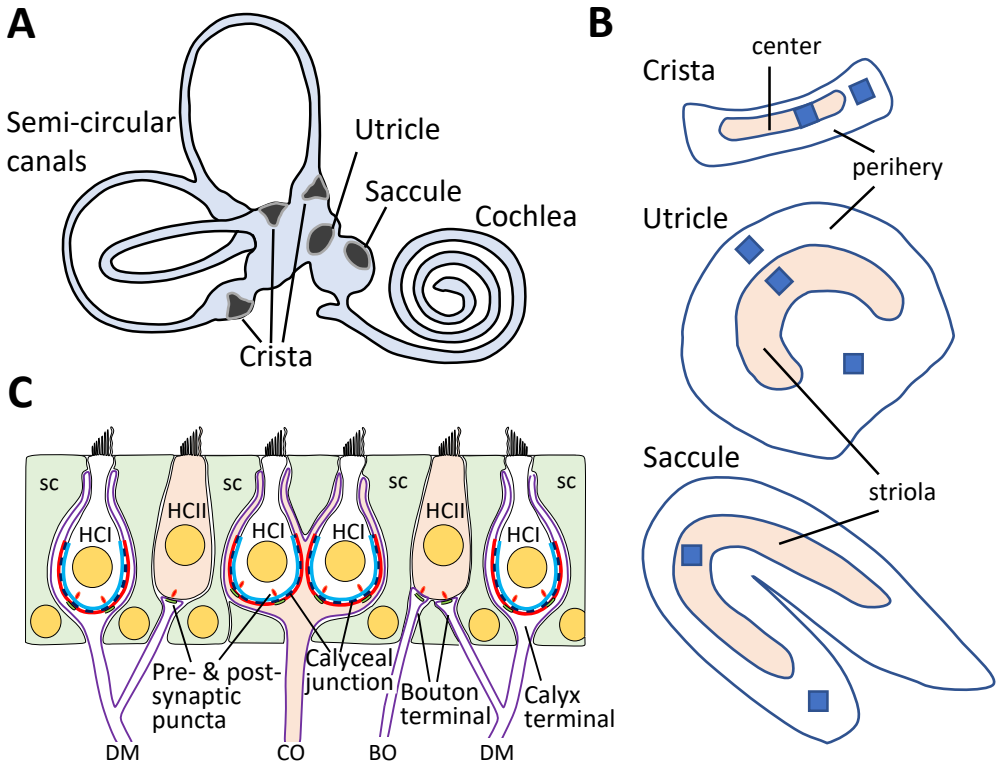
A
Semi-circular canals
Utricle
Saccule
Cochlea
Crista
B
Crista
center
perihery
Utricle
Saccule
striola
C
sc
HCI
HCII
Pre- & post-synaptic puncta
Calyceal junction
Bouton terminal
Calyx terminal
DM
CO
BO

Figure 2

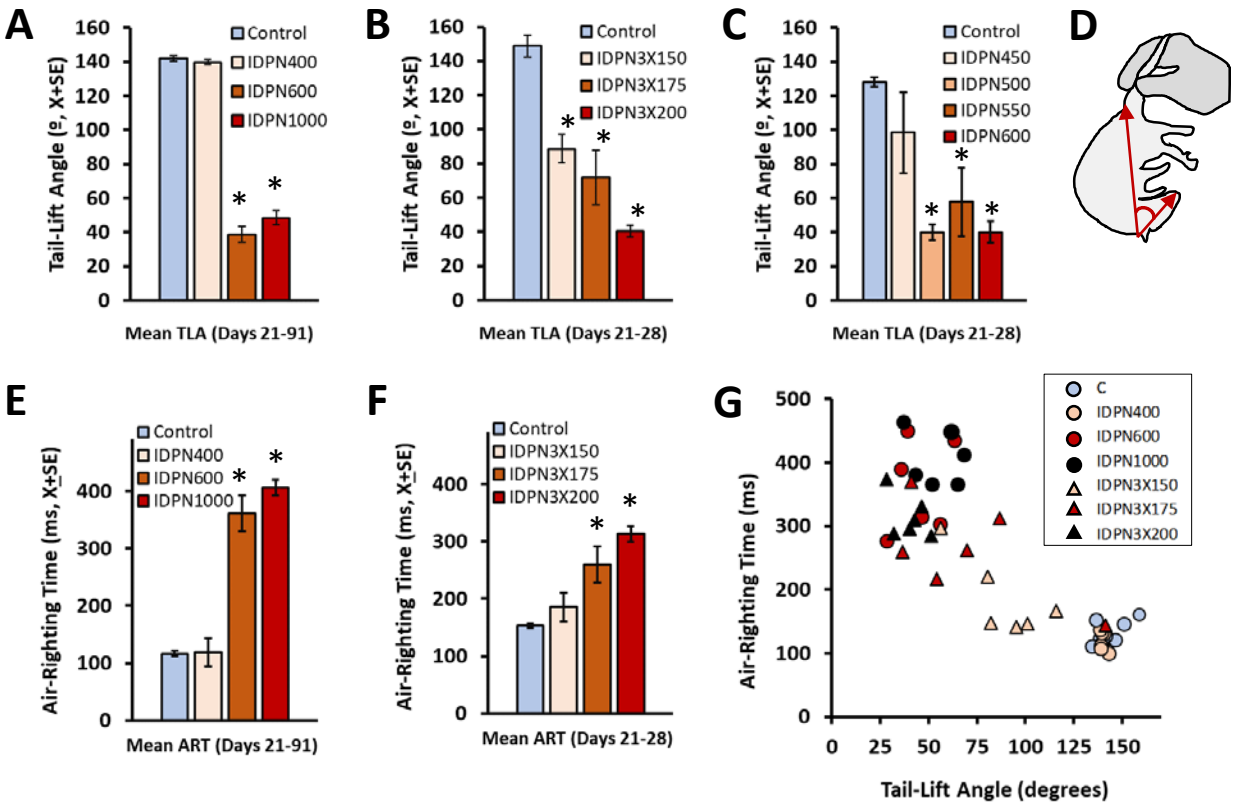
A
Tail-Lift Angle (º, X+SE)
Mean TLA (Days 21-91)
Control
IDPN400
IDPN600
IDPN1000
B
Tail-Lift Angle (º, X+SE)
Mean TLA (Days 21-28)
Control
IDPN3X150
IDPN3X175
IDPN3X200
C
Tail-Lift Angle (º, X+SE)
Mean TLA (Days 21-28)
Control
IDPN450
IDPN500
IDPN550
IDPN600
D
E
Air-Righting Time (ms, X+SE)
Mean ART (Days 21-91)
Control
IDPN400
IDPN600
IDPN1000
F
Air-Righting Time (ms, X+SE)
Mean ART (Days 21-28)
Control
IDPN3X150
IDPN3X175
IDPN3X200
G
Air-Righting Time (ms)
Tail-Lift Angle (degrees)
C
IDPN400
IDPN600
IDPN1000
IDPN3X150
IDPN3X175
IDPN3X200

Figure 3

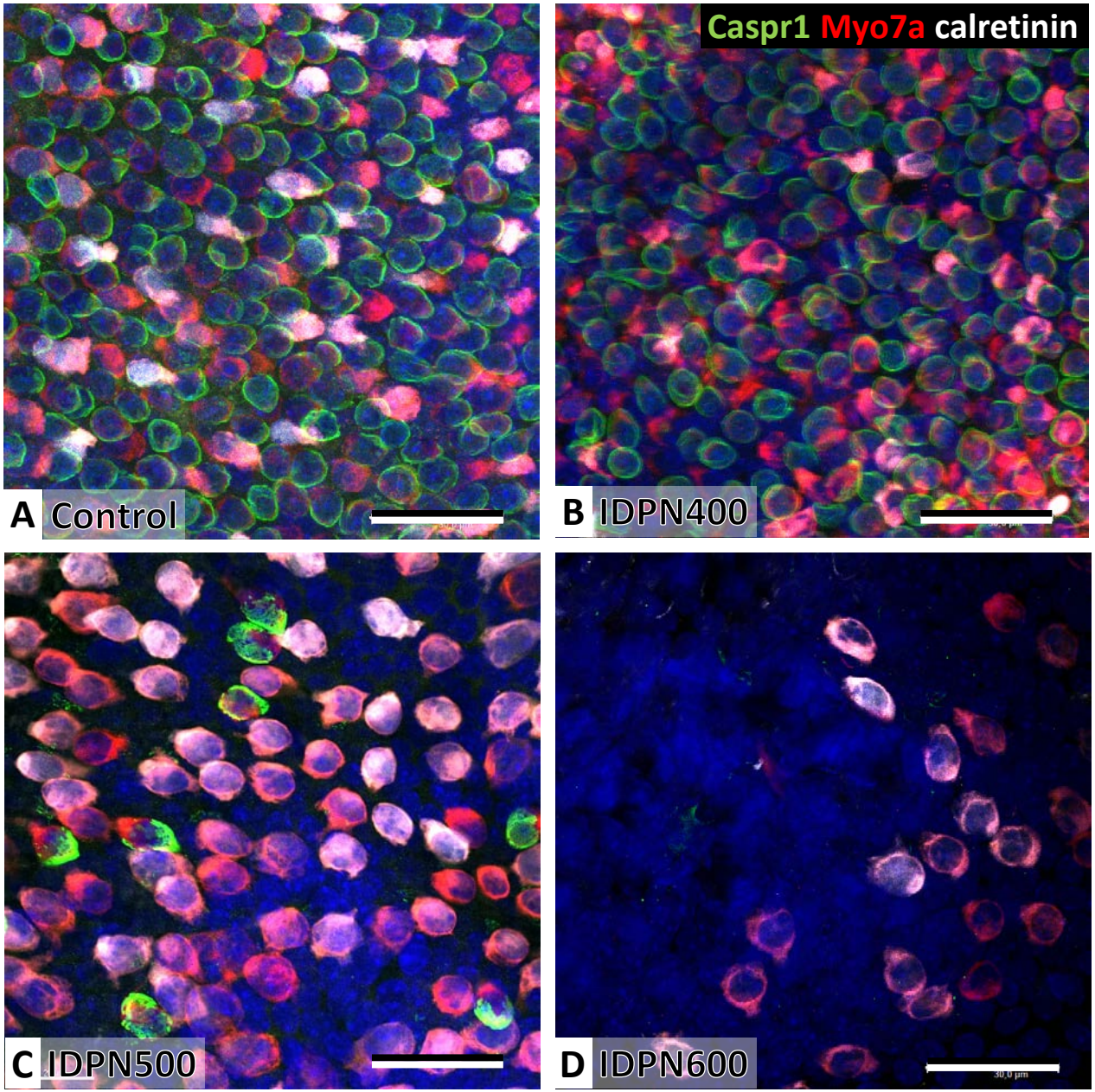
Caspr1 Myo7a calretinin
A Control
B IDPN400
C IDPN500
D IDPN600

Figure 4

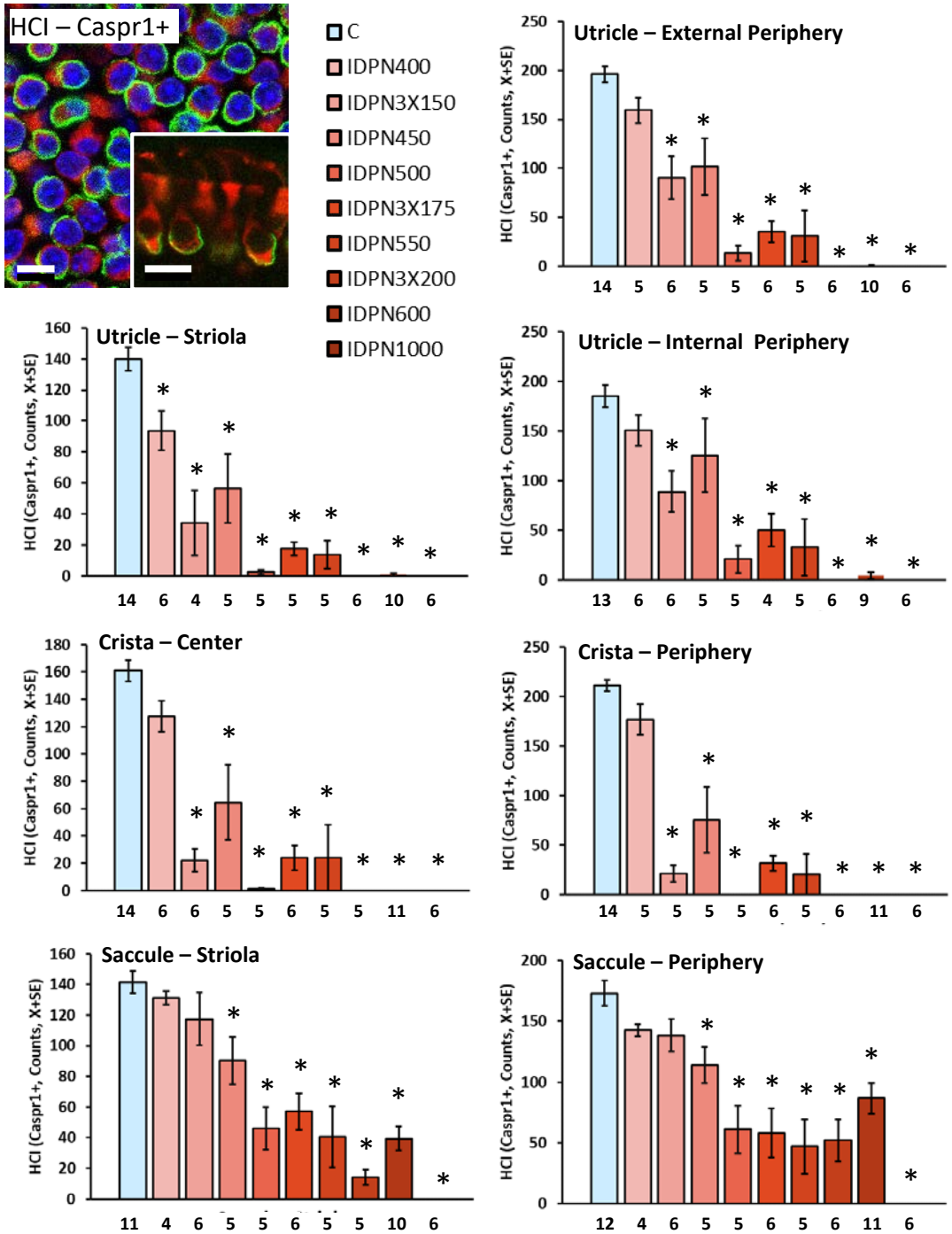
HCl – Caspr1+
C
IDPN400
IDPN3X150
IDPN450
IDPN500
IDPN3X175
IDPN550
IDPN3X200
IDPN600
IDPN1000
Utricle – External Periphery
Utricle – Striola
Utricle – Internal Periphery
Crista – Center
Crista – Periphery
Saccule – Striola
Saccule – Periphery
HCl (Caspr1+, Counts, X+SE)
14 5 6 5 5 6 5 6 10 6
14 6 4 5 5 5 5 6 10 6
13 6 6 5 5 4 5 6 9 6
14 6 6 5 5 6 5 5 11 6
14 5 5 5 5 6 5 6 11 6
11 4 6 5 5 6 5 5 10 6
12 4 6 5 5 6 5 6 11 6

Figure 5

HCII – Myo7a+/Calre+

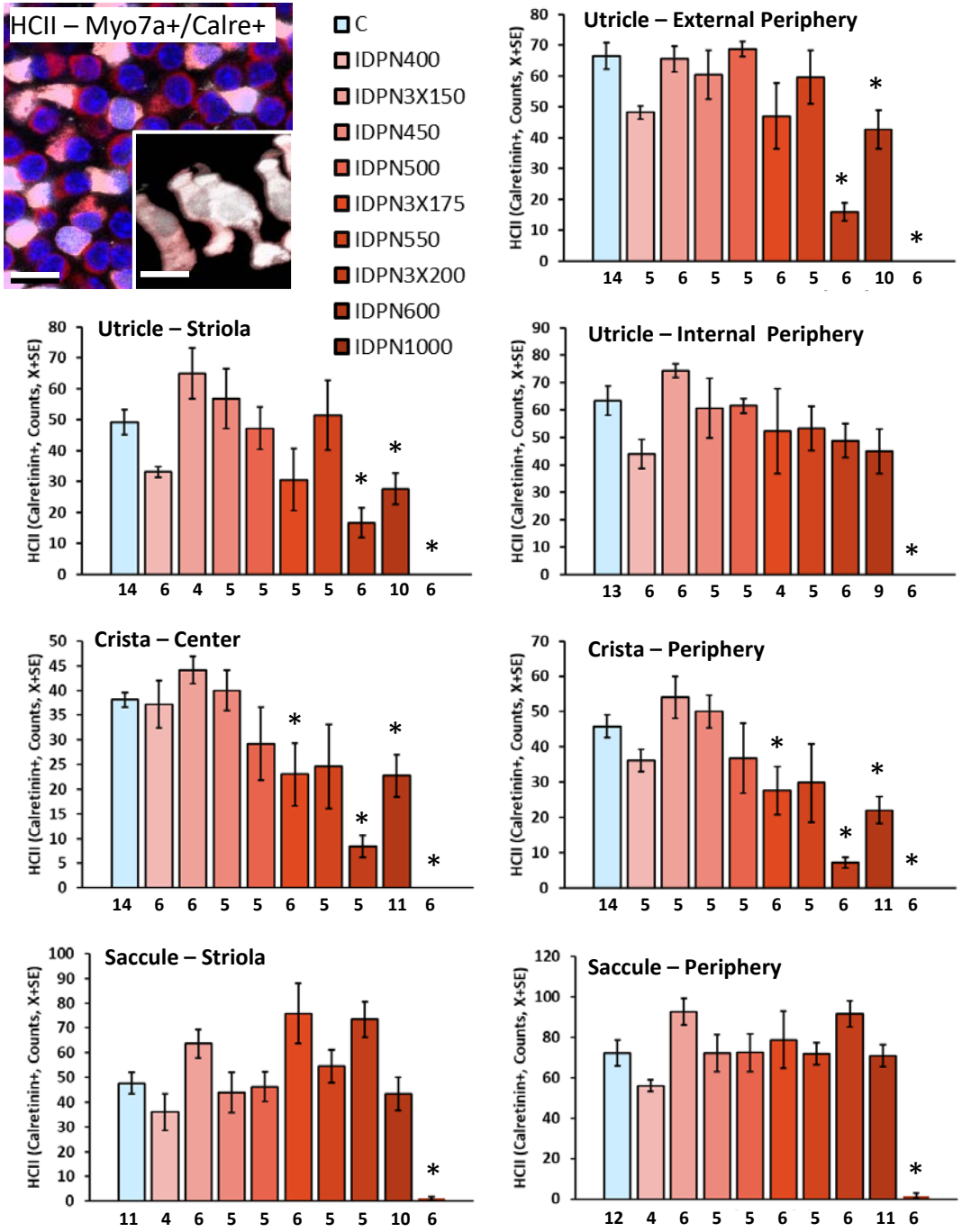
C
IDPN400
IDPN3X150
IDPN450
IDPN500
IDPN3X175
IDPN550
IDPN3X200
IDPN600
IDPN1000
Utricle – External Periphery
Utricle – Striola
Utricle – Internal Periphery
Crista – Center
Crista – Periphery
Saccule – Striola
Saccule – Periphery
HCII (Calretinin+, Counts, X+SE)
14 5 6 5 5 6 5 6 10 6
14 6 4 5 5 5 5 6 10 6
13 6 6 5 5 4 5 6 9 6
14 6 6 5 5 6 5 5 11 6
14 5 5 5 5 6 5 6 11 6
11 4 6 5 5 6 5 5 10 6
12 4 6 5 5 6 5 6 11 6

Figure 6

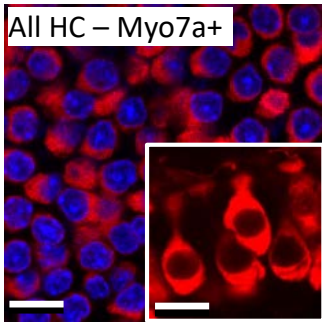

C
IDPN400
IDPN3X150
IDPN450
IDPN500
IDPN3X175
IDPN550
IDPN3X200
IDPN600
IDPN1000

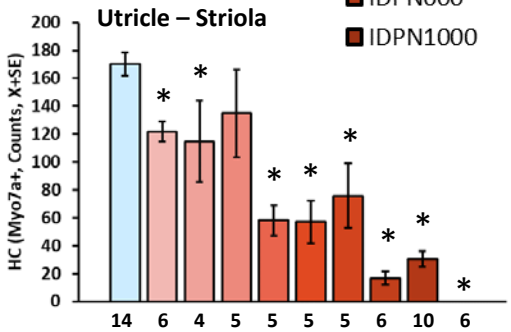

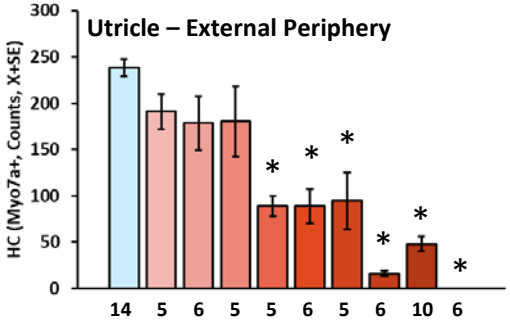

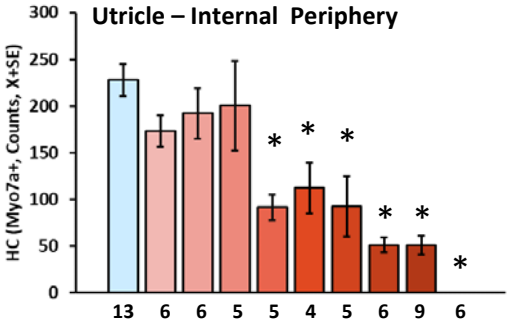

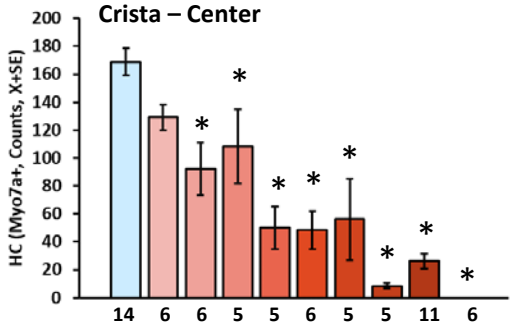

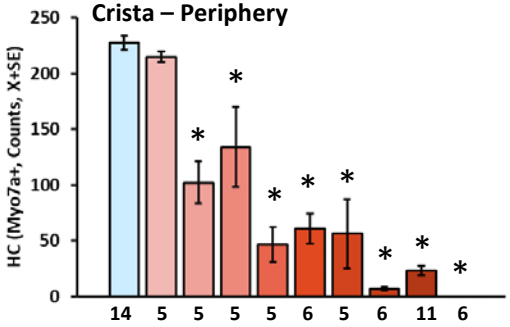

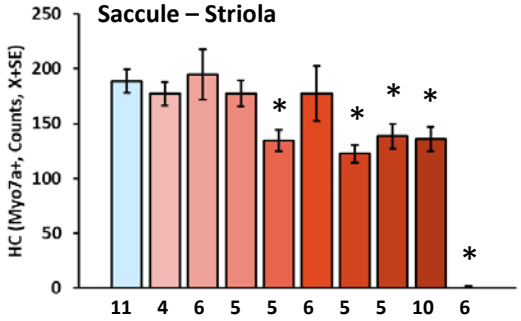

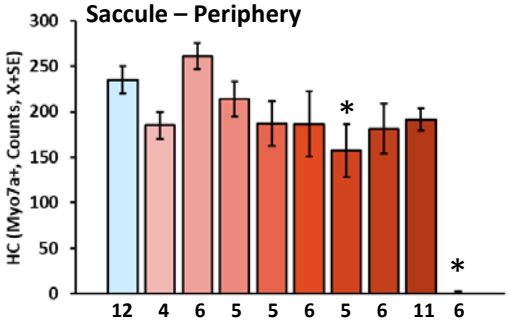

Figure 7

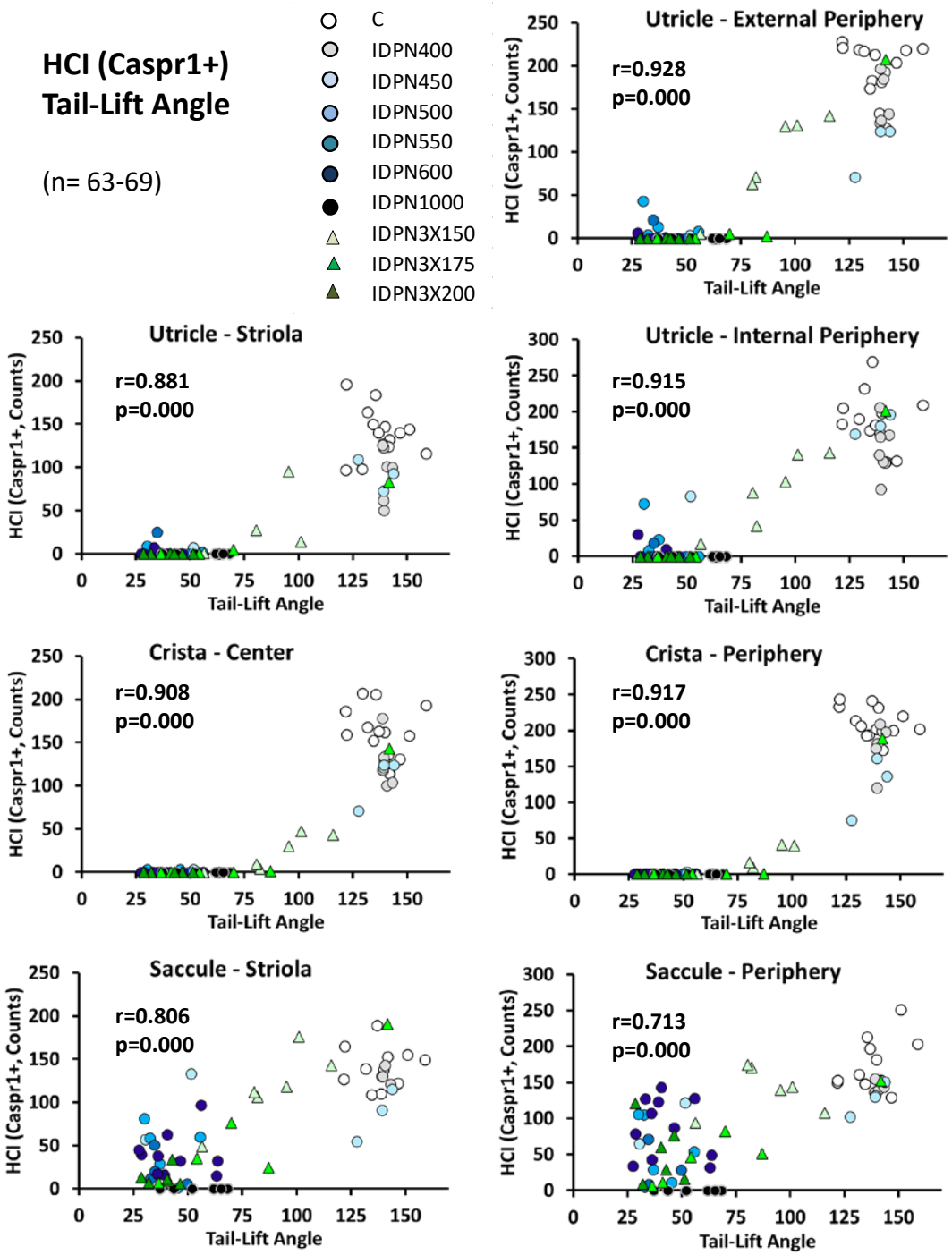
HCI (Caspr1+)
Tail-Lift Angle
(n= 63-69)
C
IDPN400
IDPN450
IDPN500
IDPN550
IDPN600
IDPN1000
IDPN3X150
IDPN3X175
IDPN3X200
Utricle - External Periphery
r=0.928
p=0.000
Utricle - Striola
r=0.881
p=0.000
Utricle - Internal Periphery
r=0.915
p=0.000
Crista - Center
r=0.908
p=0.000
Crista - Periphery
r=0.917
p=0.000
Saccule - Striola
r=0.806
p=0.000
Saccule - Periphery
r=0.713
p=0.000
HCI (Caspr1+, Counts)
Tail-Lift Angle

Figure 8

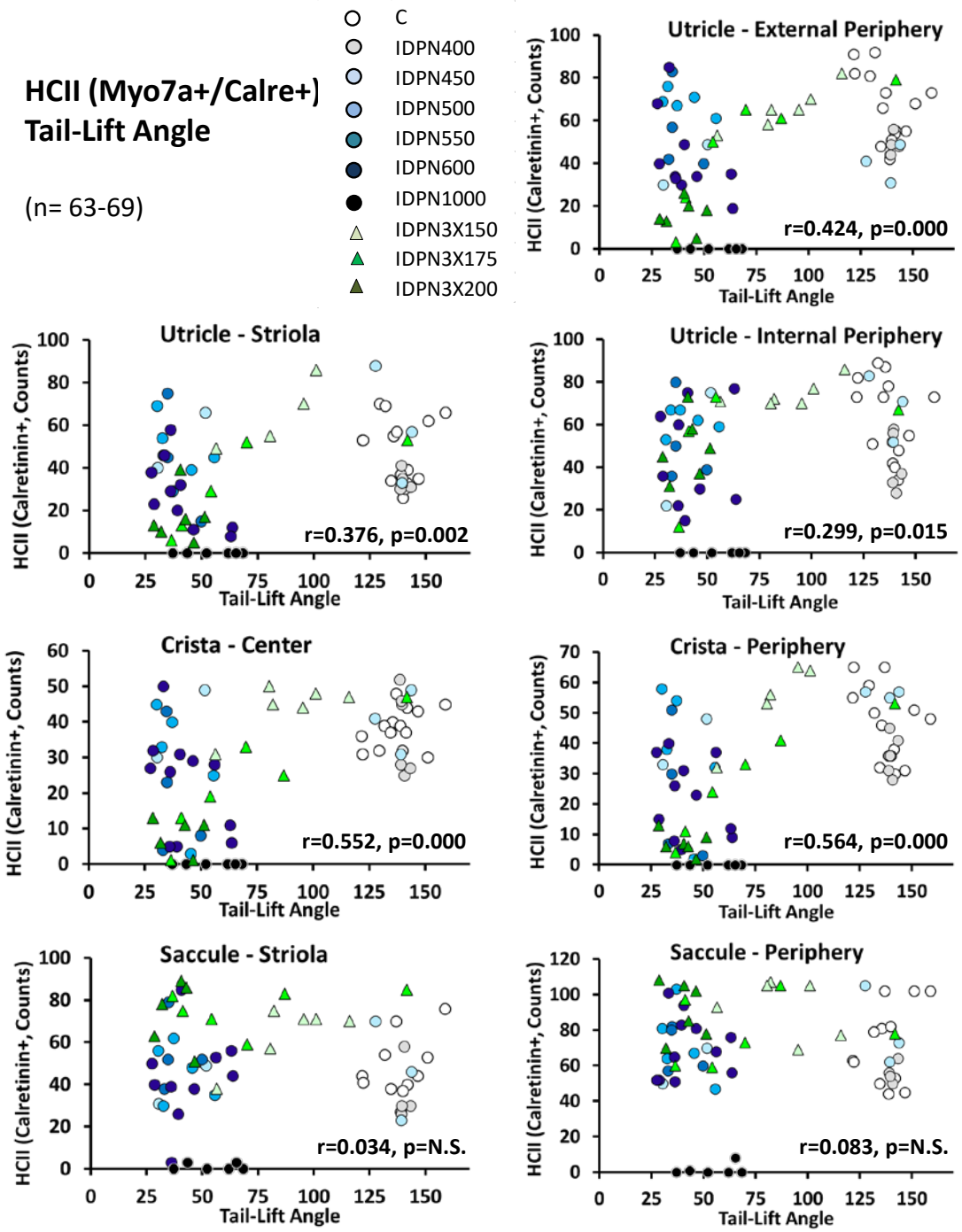
HCII (Myo7a+/Calre+)
Tail-Lift Angle
(n= 63-69)
C
IDPN400
IDPN450
IDPN500
IDPN550
IDPN600
IDPN1000
IDPN3X150
IDPN3X175
IDPN3X200
Utricle - External Periphery
r=0.424, p=0.000
Utricle - Striola
r=0.376, p=0.002
Utricle - Internal Periphery
r=0.299, p=0.015
Crista - Center
r=0.552, p=0.000
Crista - Periphery
r=0.564, p=0.000
Saccule - Striola
r=0.034, p=N.S.
Saccule - Periphery
r=0.083, p=N.S.
HCII (Calretinin+, Counts)
Tail-Lift Angle

Figure 9

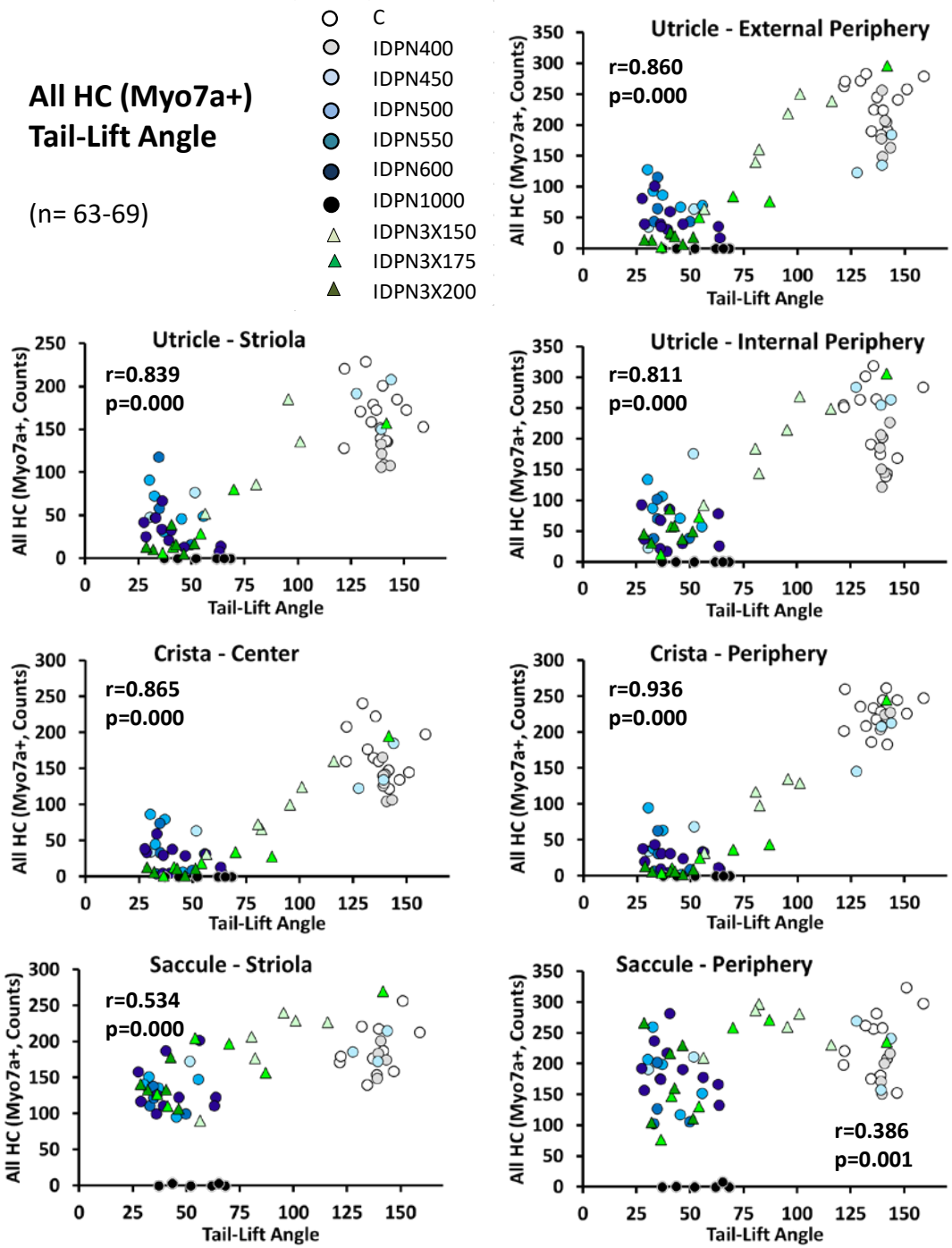
All HC (Myo7a+)
Tail-Lift Angle
(n= 63-69)
C
IDPN400
IDPN450
IDPN500
IDPN550
IDPN600
IDPN1000
IDPN3X150
IDPN3X175
IDPN3X200
Utricle - External Periphery
r=0.860
p=0.000
Utricle - Striola
r=0.839
p=0.000
Utricle - Internal Periphery
r=0.811
p=0.000
Crista - Center
r=0.865
p=0.000
Crista - Periphery
r=0.936
p=0.000
Saccule - Striola
r=0.534
p=0.000
Saccule - Periphery
r=0.386
p=0.001
All HC (Myo7a+, Counts)
Tail-Lift Angle

Figure 10

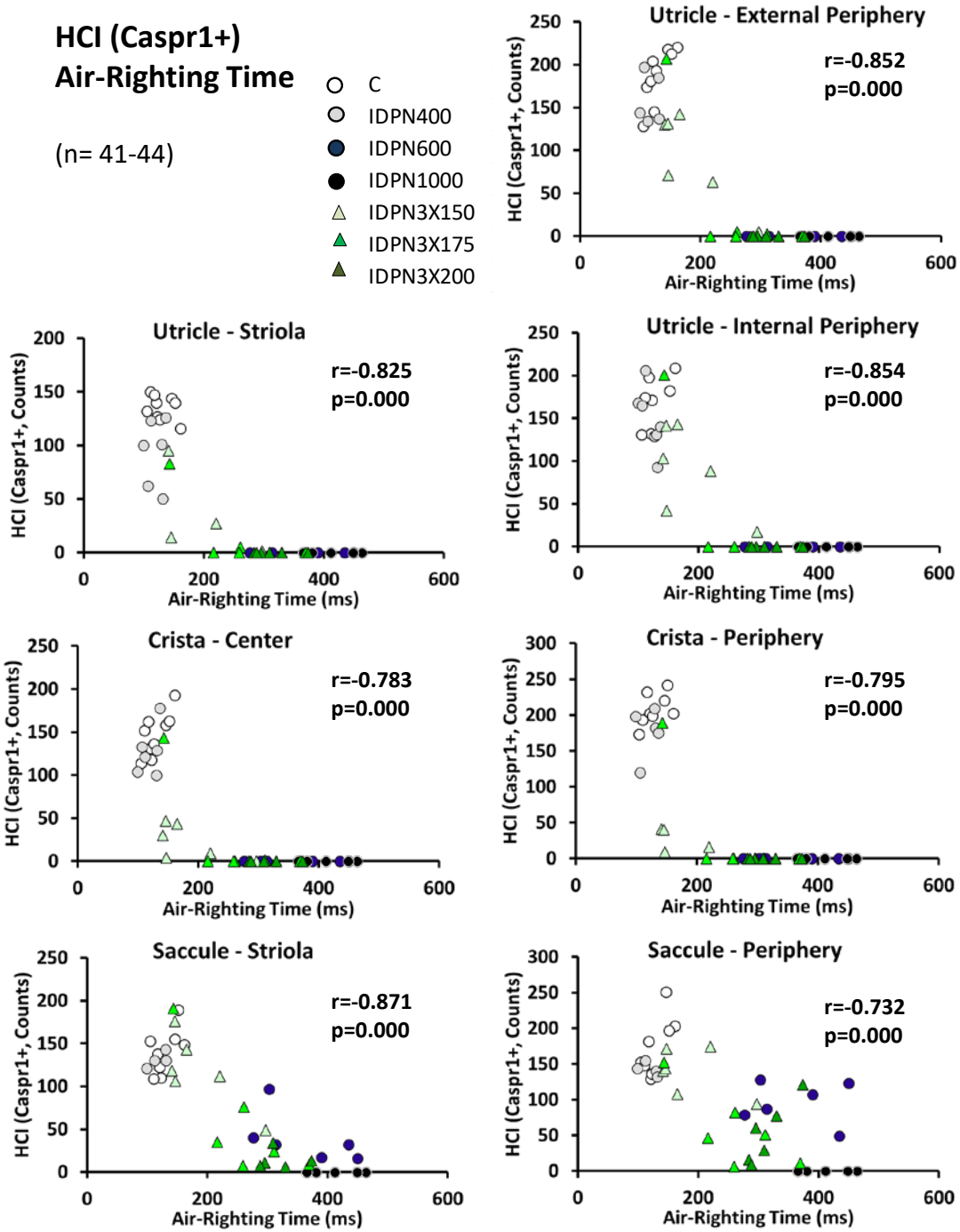
HCI (Caspr1+)
Air-Righting Time
(n= 41-44)
C
IDPN400
IDPN600
IDPN1000
IDPN3X150
IDPN3X175
IDPN3X200
Utricle - External Periphery
r=-0.852
p=0.000
Utricle - Striola
r=-0.825
p=0.000
Utricle - Internal Periphery
r=-0.854
p=0.000
Crista - Center
r=-0.783
p=0.000
Crista - Periphery
r=-0.795
p=0.000
Saccule - Striola
r=-0.871
p=0.000
Saccule - Periphery
r=-0.732
p=0.000
HCI (Caspr1+, Counts)
Air-Righting Time (ms)

Figure 11

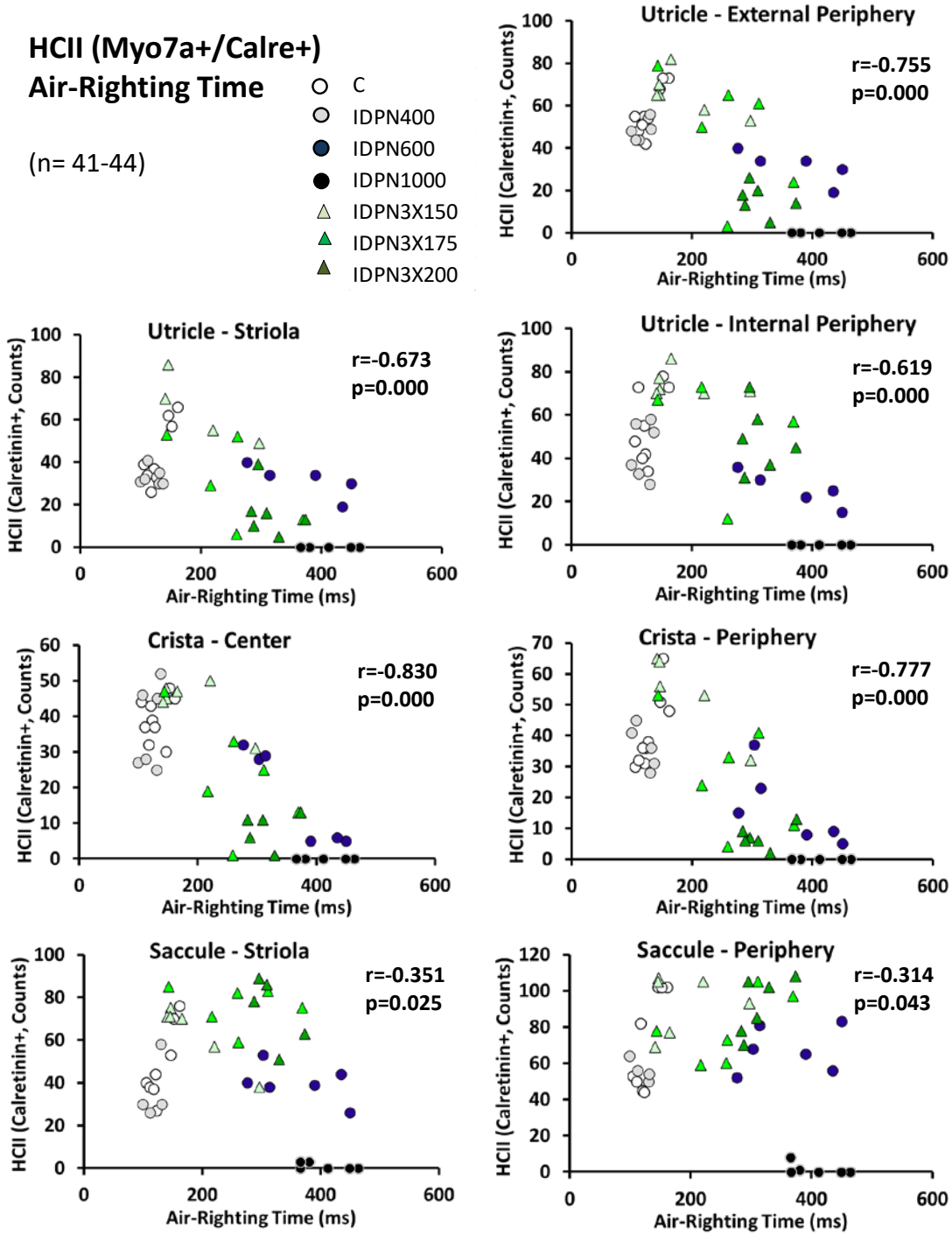
HCII (Myo7a+/Calre+)
Air-Righting Time
(n= 41-44)
C
IDPN400
IDPN600
IDPN1000
IDPN3X150
IDPN3X175
IDPN3X200
Utricle - External Periphery
r=-0.755
p=0.000
Utricle - Striola
r=-0.673
p=0.000
Utricle - Internal Periphery
r=-0.619
p=0.000
Crista - Center
r=-0.830
p=0.000
Crista - Periphery
r=-0.777
p=0.000
Saccule - Striola
r=-0.351
p=0.025
Saccule - Periphery
r=-0.314
p=0.043
HCII (Calretinin+, Counts)
Air-Righting Time (ms)

Figure 12

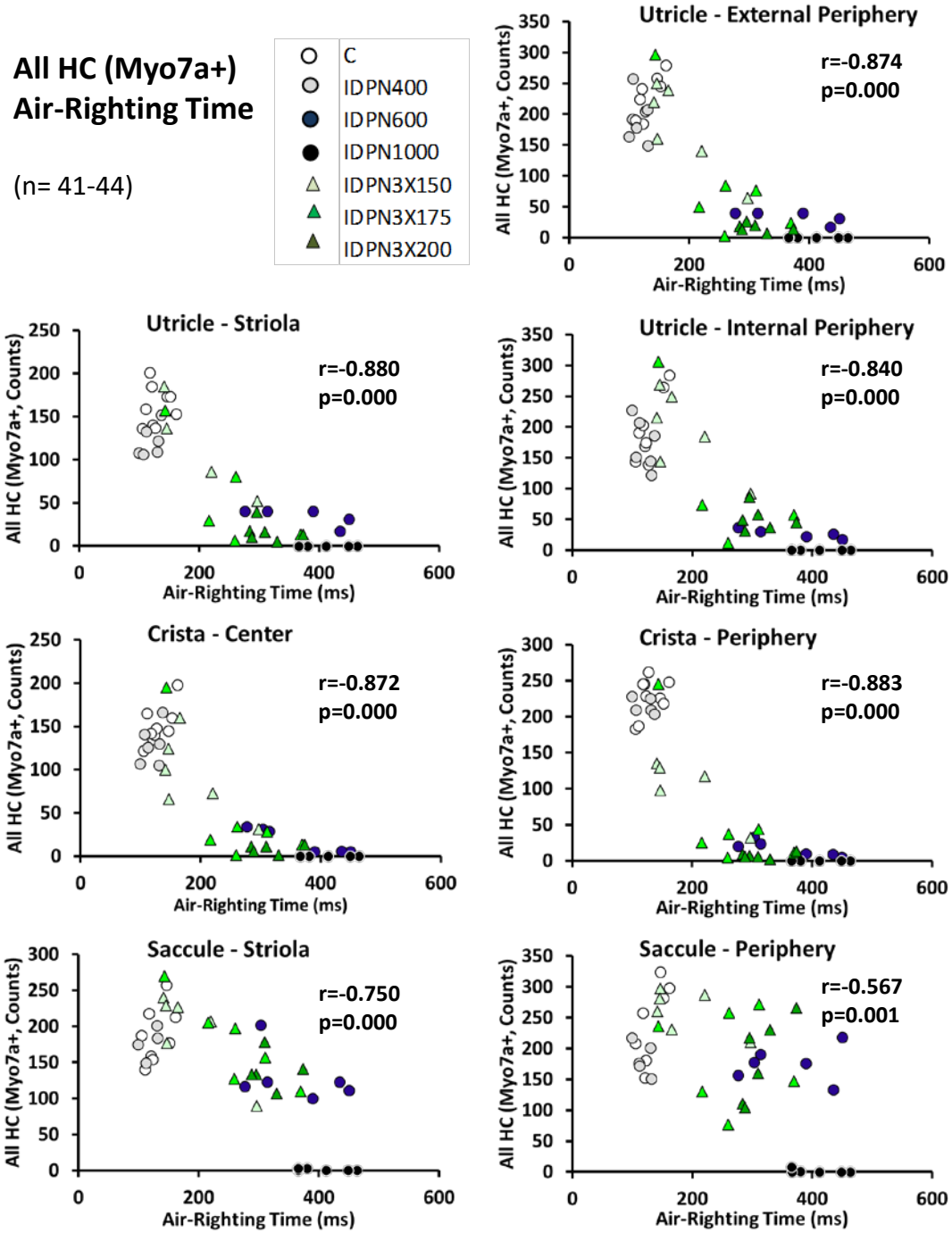
All HC (Myo7a+)
Air-Righting Time
(n= 41-44)
C
IDPN400
IDPN600
IDPN1000
IDPN3X150
IDPN3X175
IDPN3X200
Utricle - External Periphery
r=-0.874
p=0.000
Utricle - Striola
r=-0.880
p=0.000
Utricle - Internal Periphery
r=-0.840
p=0.000
Crista - Center
r=-0.872
p=0.000
Crista - Periphery
r=-0.883
p=0.000
Saccule - Striola
r=-0.750
p=0.000
Saccule - Periphery
r=-0.567
p=0.001
All HC (Myo7a+, Counts)
Air-Righting Time (ms)